

# An Empirical Ultra Wideband Channel Model for Indoor Laboratory Environments

*Narges NOORI, Roghieh KARIMZADEH-BAEE, Ali ABOLGHASEMI*

Iran Telecommunication Research Center, PO Box 14155-3961, End of North Kaargar St., Tehran, Iran

{nnoori, rkbaee, ali\_abl}@itrc.ac.ir

**Abstract.** Channel measurement and modeling is an important issue when designing ultra wideband (UWB) communication systems. In this paper, the results of some UWB time-domain propagation measurements performed in modern laboratory (Lab) environments are presented. The Labs are equipped with many electronic and measurement devices which make them different from other indoor locations like office and residential environments. The measurements have been performed for both line of sight (LOS) and non-LOS (NLOS) scenarios. The measurement results are used to investigate large-scale channel characteristics and temporal dispersion parameters. The clustering Saleh-Valenzuela (S-V) channel impulse response (CIR) parameters are investigated based on the measurement data. The small-scale amplitude fading statistics are also studied in the environment. Then, an empirical model is presented for UWB signal transmission in the Lab environment based on the obtained results.

## Keywords

Ultra wideband measurement, propagation channel, path loss, temporal dispersion parameters, clustering channel model, small-scale amplitude fading.

## 1. Introduction

The use of ultra wideband (UWB) technology has recently attracted the intense interest of wireless system designers due to its potential in short range high data rate communications [1], [2]. According to the modern definition, any signal with a bandwidth wider than 500 MHz or a fractional bandwidth greater than 0.2 can be considered as an UWB signal. A possible technique for implementing UWB is impulse radio, which is based on transmitting extremely short (in the order of nanoseconds) low power pulses [3].

In a wireless system, the transmitted signal interacts with the physical environment in a complex manner. Therefore, the ability to accurately predict propagation characteristics of UWB signals is crucial to system design. A realistic channel model can be helpful for better understanding of the propagation mechanisms and effects. Con-

sequently, UWB channel modeling in different environments has been a subject of intense research. Due to the broad variation of the multipath propagation channel, statistical approaches are the best way to model channel properties. The results of some UWB time or frequency-domain channel measurements at home, office and hospital environments have been presented in [4]-[7] for different frequency bands and transmitter-receiver separation distances. In [8], a general model has been presented for frequency range of 3.1-10.6 GHz in a number of different environments (residential, office, outdoor line of sight (LOS), outdoor non-LOS (NLOS), farm, industrial and body area network) as well as for the frequency range below 1 GHz in office environment. This model has been presented based on the measurement and simulation of the authors and other papers in the open literature. But, some of the measurements have not covered the full frequency range. As it has been mentioned, the list of the measured environments presented in [8] is not complete and other environments can be important for specific applications.

Effective design and implementation of an UWB network in the laboratory (Lab) environments needs an accurate channel model. Actually, most of the Lab environments are equipped with many electronic and measurement devices which are located on tables. The most of these devices are made of metallic materials. Therefore, the UWB propagation mechanism in the Lab may be different from other indoor locations like office and residential environments, where the most of the furniture are made from wood and textile products.

In the present work, the results of ultra wideband time-domain measurements in the laboratory (Lab) environments are investigated to present an empirical UWB channel model. These measurements have been performed for both LOS and NLOS scenarios. In the following sections, first, the UWB time-domain measurement setup, location and procedure are described in detail. Then, the measurement data is analyzed to extract path loss and shadowing fading characteristics and temporal dispersion parameters of the channel for both measurement scenarios. The clustering Saleh-Valenzuela (S-V) channel impulse response (CIR) parameters are investigated based on the measurement data at both LOS and NLOS scenarios. Then, the small-scale amplitude fading statistics are extracted in the Lab environment for both measurement scenarios.

## 2. UWB Time-Domain Measurements

### 2.1 Measurement Setup

A diagram of the time-domain measurement setup is shown in Fig. 1. At the transmitter side, a pulse generator was used as an UWB signal source. The pulse generator produces an ultra-fast pulse with 15 ps fall time. If an impulse forming network is attached to the pulse head output, the width of the output waveform of pulse generator will be less than 50 ps. The resulted impulse wave form is shown in Fig. 2. The generator was connected to the transmitting antenna through a low loss wideband cable. The output signal of the receiving antenna was amplified by a low noise amplifier with a gain of 28 dB and 3 dB bandwidth of 12 GHz. A digital sampling oscilloscope was used at the receiver side which sampled the received signal at a rate of 1 sample per 12.5 ps. This oscilloscope has a bandwidth up to 70 GHz. The pulse generator and digital sampling oscilloscope were synchronized through a reference clock signal at a frequency of 200 kHz. Measurements were performed by a pair of 1-18 GHz double-ridged waveguide horn antennas. These transmitting and receiving antennas were both placed on moving carts at a height of 135 cm above ground. It should be noted that since the transmitting and receiving antennas are included as parts of the UWB channel (as shown in Fig. 1), the UWB time domain measurements and presented channel model are antenna dependent.

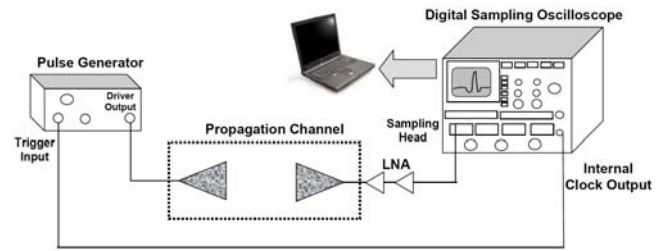


Fig. 1. A diagram of the used time-domain measurement setup.

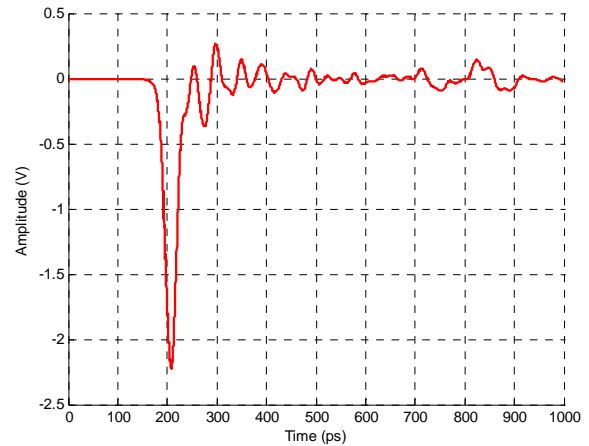


Fig. 2. Output waveform of pulse generator.

### 2.2 Measurement Location

The time-domain measurement campaign was conducted for both LOS and NLOS scenarios at a basement floor with a plan shown in Fig. 3. All the main rooms of this floor are modern Labs. The building walls are made of brick with metallic stud. The partitions are aluminum frame structured with fabric, wood and glass surface. The floor of the rooms is covered with tiles. The doors are made of wood and have metallic frames. The furniture inside each room consists of many different electronic and measurement devices, metallic and wooden cupboards and cabinets, tables made of wood, mid back work chairs, computers, etc.



Fig. 3. Plan of the measurement environment with different Tx and Rx locations.

### 2.3 Measurement Procedure

To perform the measurements, five different transmitter locations were considered. The receiver points were chosen at those locations where the received signal could be clearly detected. The measurements were collected at each receiver location by moving the receiver antenna over a square grid of 9 points spaced 50 cm apart as shown in Fig. 3. In order to cancel out the noise, 100 measurements were averaged at each measurement point. A system calibration was made to compensate any imperfection of the system components. Then, any dc offset that had not been taken into account by the calibration was removed.

## 3. Measurement Result Analysis

### 3.1 Path Loss and Large-Scale Analysis

Large-scale fading can be categorized by path loss and shadowing. To investigate UWB large-scale fading behavior, the distance dependency of the path loss which

can describe attenuation of the median power as a function of distance, is introduced as [3]:

$$PL(d) = PL(d_0) + 10\gamma \log_{10}\left(\frac{d}{d_0}\right) + \chi \quad d \geq d_0 \quad (1)$$

where  $PL(d)$  represents the path loss at a distance  $d$ ,  $PL(d_0)$  is the path loss at reference distance  $d_0$ ,  $\gamma$  is the path loss exponent and  $\chi$  is the shadowing fading parameter. This parameter shows that path loss observed at any given point will deviate from its average value. The values of  $PL(d_0)$  and  $\gamma$  can be obtained through a least square linear fit to the measured data. The reference distance is set to 1.5 m and 3.4 m for LOS and NLOS path loss model, respectively where these values are the minimum observation distances in each scenario. Thus, the path loss models are valid for distances above these reference values. The extracted parameters are  $PL(d_0) = PL(1.5 \text{ m}) = 28.71 \text{ dB}$  and  $\gamma = 1.81$  for LOS scenario and  $PL(d_0) = PL(3.4 \text{ m}) = 39.16 \text{ dB}$  and  $\gamma = 3.45$  for NLOS scenario. The scatter plots of the path loss versus the transmitter-receiver separation distance are shown in Fig. 4 for both scenarios.

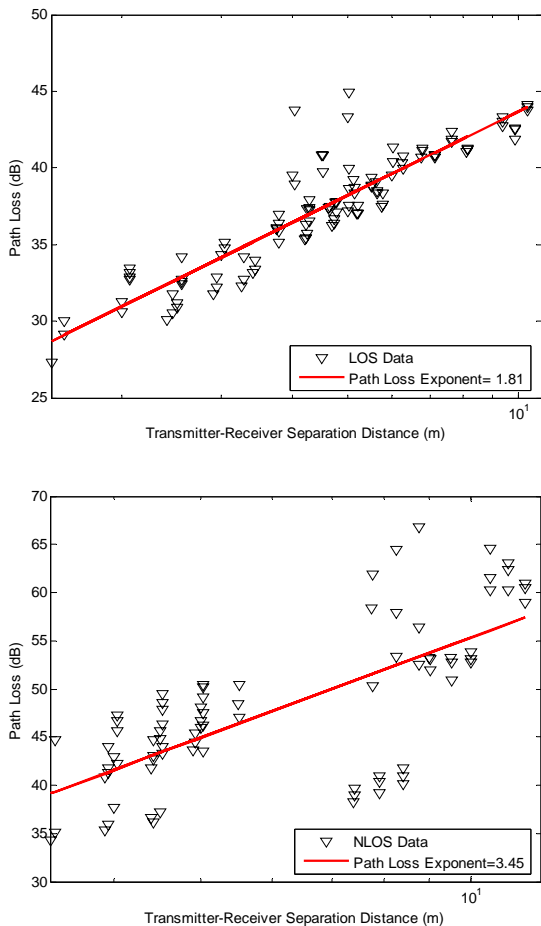


Fig. 4. Scatter plots of the path loss versus the transmitter-receiver separation distance.

The shadowing fading parameter is a zero-mean Gaussian distributed random variable in dB with standard deviation  $\sigma_\chi$  which is also in dB. The standard deviation of

the shadowing fading parameter is found by calculating deviation from the obtained fit. Based on our measurements, the values of  $\sigma_\chi$  are 1.62 dB and 5.71 dB for LOS and NLOS scenarios, respectively. A comparison of the theoretical cumulative distribution function (CDF) of a zero-mean Gaussian random variable with the empirical CDF of the shadowing fading parameter is shown in Fig. 5 for both LOS and NLOS scenarios.

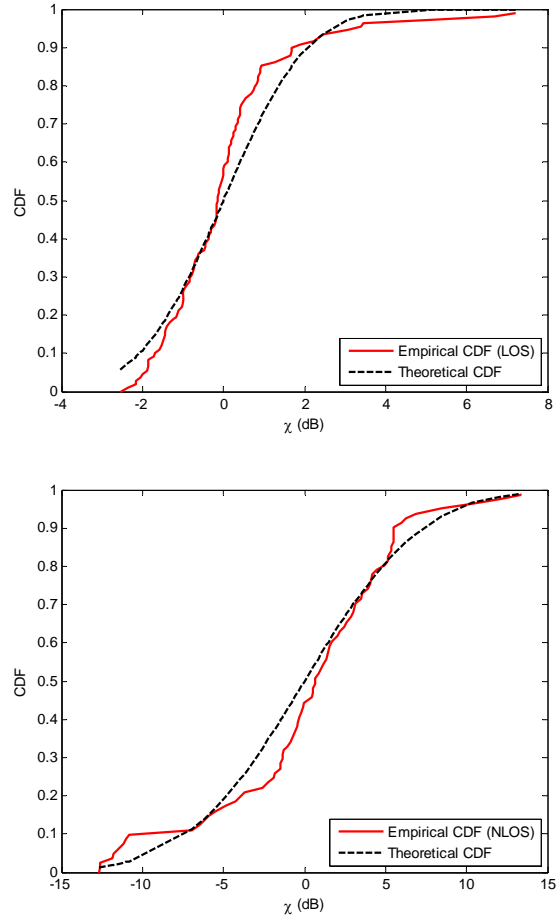


Fig. 5. A comparison of the theoretical CDF of a zero-mean Gaussian random variable with empirical CDF of the shadowing fading parameter.

### 3.2 Temporal Dispersion Results

In a wireless system, the signal arriving at a receiver point is in general a summation of several multipath components (MPCs). The power delay profile (PDP) provides an indication of dispersion of the transmitted power over various paths. The channel temporal dispersion characteristics show temporal distribution of the power relative to the first arriving component. These characteristics are usually quantified in terms of the mean excess delay and RMS delay spread. To obtain these parameters, the power delay profile is normalized and all signals below a specific threshold  $x$  dB relative to the maximum are forced to zero [9]. This is done to remove the noise that varies from one measurement setup to another.

The mean excess delay,  $\tau_m$ , is defined as the first moment of the PDP [10]

$$\tau_m = \frac{\sum_k P(\tau_k) \tau_k}{\sum_k P(\tau_k)}. \quad (2)$$

The RMS delay spread is the square root of the second central moment of the power delay profile [10]

$$\tau_{RMS} = \sqrt{\tau_m^2 - (\tau_m)^2} \quad (3)$$

where

$$\tau_m^2 = \frac{\sum_k P(\tau_k) \tau_k^2}{\sum_k P(\tau_k)}. \quad (4)$$

We use a 20 dB threshold to calculate the delay spread parameters. The resulted mean excess delay is varied between 0.45 ns and 17.64 ns in LOS conditions and between 0.75 ns and 25.73 ns in NLOS conditions. The CDF of the RMS delay spread is plotted in Fig. 6 for both measurement scenarios. This figure shows that the most probable values of RMS delay spread are around 2.7 ns and 4.7 ns for LOS and NLOS scenarios, respectively. The obtained parameter values indicate that the channel suffers from higher temporal dispersion in NLOS conditions.

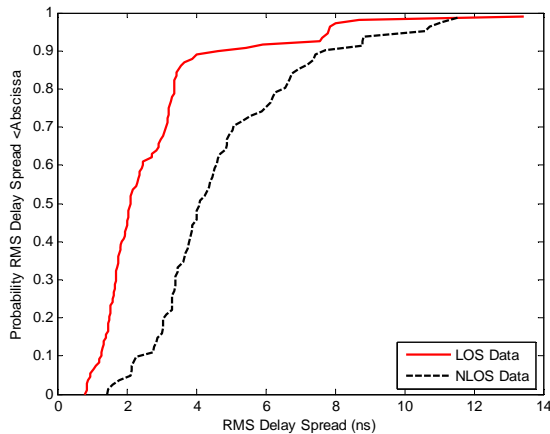


Fig. 6. Cumulative distribution functions for the RMS delay spread (20 dB).

Another important parameter which can be used to evaluate temporal dispersion characteristics of the channel is the ratio of mean excess delay to RMS delay spread. The lower values of this ratio indicate high concentration of the power at small values of the mean excess delay; while, the higher values of this ratio indicate high concentration of the power at larger values of the mean excess delay [5, 6, 9]. The relation between the mean excess delay and RMS delay spread for both LOS and NLOS scenarios is shown in Fig. 7. The best least square linear fit to the measured data gives the values of 1.40 and 2.67 for this ratio in LOS and NLOS conditions, respectively. This means that in LOS conditions, the power is more concentrated at the received components with lower time delay values, while in NLOS conditions, the power is more concentrated at the received components with higher time delay values.

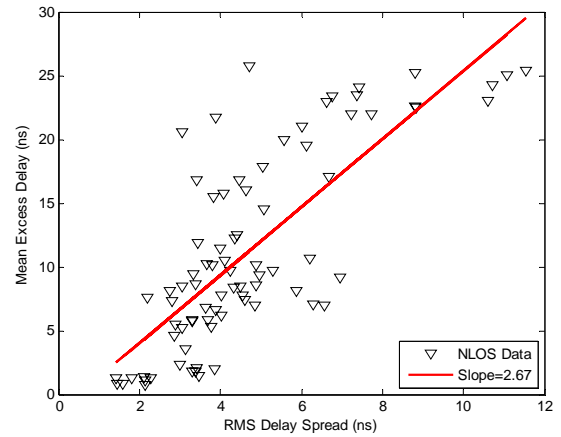
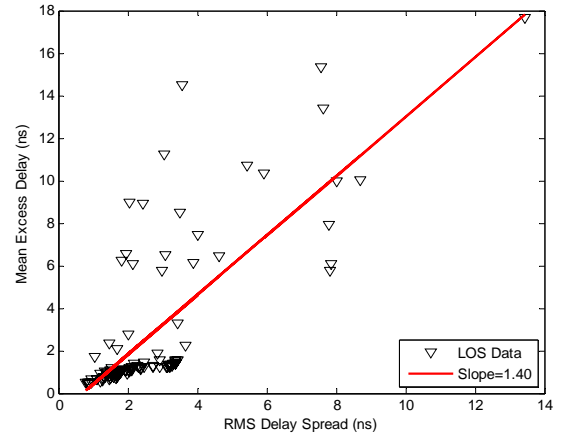


Fig. 7. Scatter plots for the mean excess delay versus RMS delay spread.

### 3.3 Clustering Channel Model

As it is reported in most of the UWB measurement campaigns, the arriving MPCs tend to form clusters in the temporal domain [11]-[13]. An UWB channel impulse response (CIR) which account for the clustering phenomenon of MPCs has been proposed in [13] based on the conventional Saleh-Valenzuela (S-V) channel model [14], where the model parameters have been derived using measurement data collected in the frequency band of 3-10 GHz in various types of high-rise apartment under different propagation scenarios.

The clustering CIR of the UWB channel can be expressed by S-V model as follows [13]:

$$h(t) = \sum_{l=0}^L \sum_{k=0}^{K_l} a_{k,l} \delta(t - T_l - \tau_{k,l}) \quad (5)$$

where  $\delta(\cdot)$  is the Dirac delta function,  $L$  is the number of clusters,  $K_l$  is the number of MPCs within the  $l$ th cluster,  $a_{k,l}$  is the multipath gain coefficient of the  $k$ th component in the  $l$ th cluster,  $T_l$  is the delay of the  $l$ th cluster which is defined as the time of arrival of the first arriving MPC within the  $l$ th cluster and  $\tau_{k,l}$  is the delay of the  $k$ th MPC relative to the  $l$ th cluster arrival time,  $T_l$ . From (5),  $\{L, T_l\}$  and  $\{K_l, \tau_{k,l}, a_{k,l}\}$  are classified as inter-cluster and intra-

cluster parameters, respectively [13]. The number of clusters,  $L$ , is modeled by a Poisson distribution as proposed in [15]. The presence of some objects in the environment under consideration can increase the number of clusters. It was found that the number of MPCs per cluster,  $K_i$ , can be modeled by exponential distribution. It should be noted that the number of MPCs per cluster (thus, the number of clusters) is dependent on the resolution of the parameter estimation technique, the type of the transmitting and receiving antennas, the transmitter-receiver separation distance, the physical layout of the environment and the dynamic range of the measurement system. More clusters are observed in a heavily cluttered environment.

Based on the S-V channel model, the cluster inter-arrival times and the ray intra-arrival times are described by two independent exponential probability density functions as follows [14]:

$$p(T_i | T_{i-1}) = \Lambda \exp[-\Lambda(T_i - T_{i-1})] \quad l > 0 \quad (6)$$

$$p(\tau_{k,l} | \tau_{(k-1),l}) = \lambda \exp[-\lambda(\tau_{k,l} - \tau_{(k-1),l})] \quad k > 0 \quad (7)$$

where  $\Lambda$  is the mean cluster arrival rate and  $\lambda$  is the mean ray arrival rate.

The average power of both clusters and rays within the clusters are assumed to decay exponentially:

$$\overline{a_{k,l}^2} = \overline{a_{0,0}^2} e^{-T_k/\Gamma} e^{-\tau_{k,l}/\gamma} \quad (8)$$

where  $\overline{a_{0,0}^2}$  is the expected value of the power of the first arriving MPC,  $\Gamma$  is the decay exponent of the clusters and  $\gamma$  is the decay exponent of the rays within the clusters.

From analysis of the recorded measurements in the Lab environment, the average number of clusters,  $\bar{L}$ , is obtained equal to 2.3 and 2.9 for LOS and NLOS scenarios, respectively. The resulted cumulative distribution functions (CDFs) of the number of MPCs per cluster,  $K_i$ , are shown in Fig. 8 for both scenarios. As can be seen in this figure, the CDFs can be closely modeled by theoretical exponential distribution functions with the mean value of  $\mu_{K_i}$ , which is equal to 32.7 and 81.5 for LOS and NLOS scenarios, respectively. It can be seen that the mean value of the number of MPCs per cluster is increased from LOS to NLOS scenarios.

In order to extract the mean cluster arrival rate,  $\Lambda$ , the arrival time of the first MPC in each cluster was considered to be the cluster arrival time, regardless of whether or not it had the largest amplitude. The arrival time of each cluster was subtracted from its successor. The conditional probability distribution given in (6) could be estimated by applying the least mean square fit of the cluster inter-arrival time to an exponential distribution. The resulted  $1/\Lambda$  values are 7.95 ns and 12.49 ns for LOS and NLOS scenarios, respectively. A similar method should be carried out to estimate  $\lambda$  which is the average ray arrival rate within a cluster. The estimated  $1/\lambda$  values are 1.03 s and 1.06 ns in LOS and NLOS conditions, respectively.

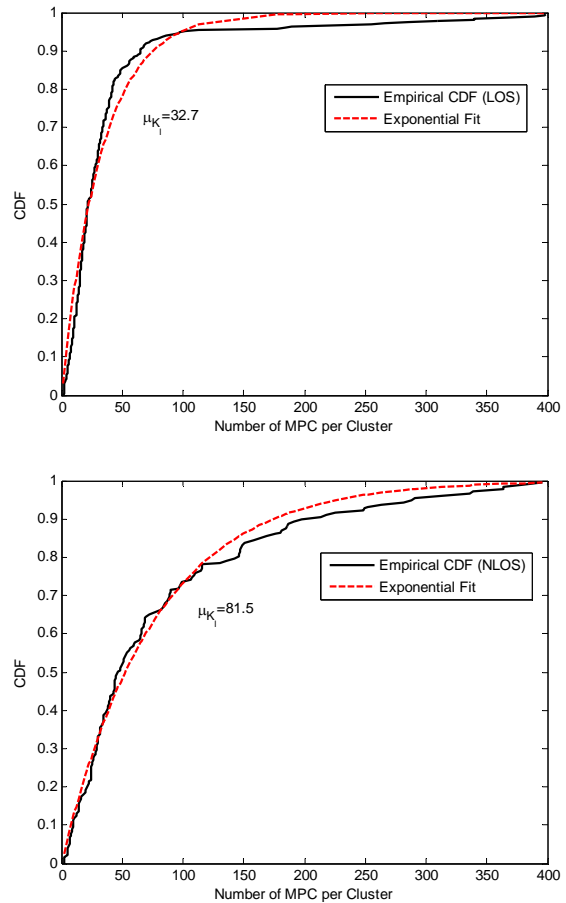


Fig. 8. CDFs of the number of MPCs per cluster for LOS and NLOS scenarios.

| Parameter        | LOS scenario | NLOS scenario |
|------------------|--------------|---------------|
| $\bar{L}$        | 2.3          | 2.9           |
| $\mu_{K_i}$      | 32.7         | 81.5          |
| $\Gamma$ (ns)    | 22.1         | 34.6          |
| $\gamma$ (ns)    | 11.3         | 16.3          |
| $1/\Lambda$ (ns) | 7.95         | 12.49         |
| $1/\lambda$ (ns) | 1.03         | 1.06          |

Tab. 1. Parameters of the clustering S-V channel model for LOS and NLOS scenarios.

The cluster and ray decay exponents,  $\Gamma$  and  $\gamma$ , can be estimated by considering clusters and rays with normalized amplitudes and time delays and selecting their mean decay rates. In order to estimate  $\Gamma$ , amplitude of the first cluster arrival in each data set is set to one and its time delay is set to zero. Then, all other clusters arrivals in the same data set are expressed relative to this amplitude and time. The estimates for  $\Gamma$  which obtained by the least mean square fit are 22.1 ns and 34.6 ns for LOS and NLOS scenarios, respectively. Applying a similar approach to estimate  $\gamma$  results in values of 11.3 ns and 16.3 ns for LOS and NLOS scenarios, respectively. For better comparison of the resulted model in tow scenarios, the obtained parameters are listed in Tab.1.

### 3.4 Amplitude Fading Statistics

One of the fundamental parts of the channel characterization is study of the small-scale amplitude fading. The Rice and Rayleigh distributions can describe the amplitude fading statistics in conventional narrowband channel models for LOS and NLOS condition, respectively. In UWB propagation, the wide frequency bandwidth corresponds to a high temporal resolution capability. Therefore, a single path arriving at a certain delay must be resolved. In order to evaluate the small-scale amplitude fading statistics, the empirical amplitudes over small-scale areas are calculated. Depending on the measurement environments and scenarios relative data from taps at specific excess delays were matched to some typical theoretical distributions for amplitude fading statistics such as lognormal, Nakagami, Rayleigh, Rice and Weibull distributions [3]. In [16]-[18], the lognormal distribution was obtained to give the best fit for the amplitude fading statistics, while other measurement campaigns such as [19], [20] show that the small-scale amplitude fading statistics can be modeled by the Nakagami distribution. In [21], the Rice distribution has also best fitted to empirical data. The measurement results reported in [13], [22], [23] show that the small-scale amplitude fading have a good fit with Weibull distribution in fully furnished conference rooms, modern office buildings and high rise apartments.

In order to extract small-scale amplitude fading statistics from the measurement data in the Lab environment, empirical data of the PDPs from different measurement position are gathered and classified into LOS and NLOS. Amplitudes smaller than 20 dB of the peak in each PDP are set to zero in order to get only the appropriate data for analysis. Then, data from taps at specific excess delays are collected. Each tap is assumed to contain either one resolvable path or no path. This delay tap is determined by the time resolution of the specific measurement system. In our measurement system, the delay tap width is 12.5 ps. Extraction of the amplitudes for each tap is carried out by collecting a vector of amplitude values having the same delays. It is found that these data from taps at specific excess delays can be matched to lognormal, Nakagami and Weibull distributions where the parameters of these distributions i.e. the standard deviation of the lognormal distribution, m-parameter of the Nakagami distribution and b-shape parameter of the Weibull distribution are all lognormally distributed random variables [3]. Variations of these parameters as a function of excess delay are extracted from the measurement data for both LOS and NLOS scenarios. The mean value and standard deviation of the lognormal distribution of these three parameters are listed in Tab. 2.

The Kolmogorov–Smirnov (K–S) and chi-square ( $\chi^2$ ) hypothesis tests are used to elaborate the goodness-of-fit for these candidate amplitude distributions. A significance level of 5% is used to evaluate the reliability of the fit. Tab. 3 compares the passing rate of the K-S and  $\chi^2$  tests for the above distributions. It is found that the Weibull distribution gives the highest passing rate in both tests. There-

fore, the small-scale amplitude fading statistics can be well-modeled by Weibull distribution for both scenarios. The CDFs of the empirical small-scale amplitude fading fitted to the Weibull distribution are plotted in Fig. 9 at 6 ns and 12 ns excess delays for LOS condition.

| Parameter     | $\sigma$ -Lognormal |                     | m-Nakagami |               | b-Weibull  |               |
|---------------|---------------------|---------------------|------------|---------------|------------|---------------|
|               | $\mu_{\sigma L}$    | $\sigma_{\sigma L}$ | $\mu_{mN}$ | $\sigma_{mN}$ | $\mu_{bW}$ | $\sigma_{bW}$ |
| LOS scenario  | 1.1862              | 0.1938              | 0.4886     | 0.0895        | 1.1838     | 0.2360        |
| NLOS scenario | 1.4823              | 0.2806              | 0.3855     | 0.0819        | 0.8553     | 0.1893        |

Tab. 2. Mean and standard deviation of the parameters for candidate distributions in LOS and NLOS scenarios.

| Distribution | LOS scenario |          | NLOS scenario |          |
|--------------|--------------|----------|---------------|----------|
|              | K-S          | $\chi^2$ | K-S           | $\chi^2$ |
| Lognormal    | 73.48        | 38.03    | 98.65         | 82.22    |
| Nakagami     | 69.89        | 64.44    | 35.60         | 36.55    |
| Weibull      | 97.53        | 84.17    | 99.70         | 89.43    |

Tab. 3. Passing rate of K-S and  $\chi^2$  hypothesis tests.

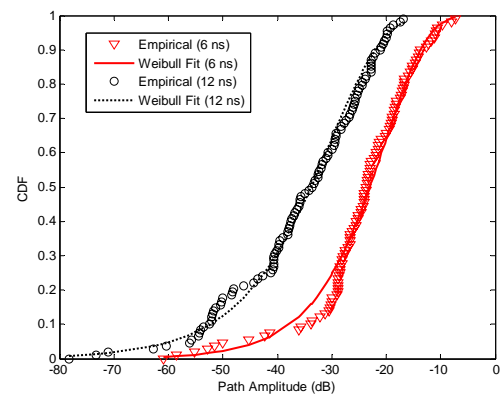


Fig. 9. CDFs of the empirical small-scale amplitude fading fitted to Weibull distribution at excess delay 6 ns and 12 ns for LOS scenario.

## 4. Conclusions

The results of time-domain UWB channel measurement in the Lab environment were presented. Both LOS and NLOS scenarios were considered and the path loss model and main temporal dispersion parameters were found. The calculated path loss exponent was 1.81 and 3.45 for LOS and NLOS scenarios, respectively. The CDF of the shadowing fading parameter was obtained. The resulted temporal dispersion parameters were also presented. The clustering CIR parameters were obtained for both LOS and NLOS scenarios and distribution functions of these parameters were investigated in the measurement environment. The small-scale amplitude fading statistics were extracted for both LOS and NLOS conditions. It was shown that small-scale amplitude fading can be modeled by the lognormal, Nakagami and Weibull distributions but Weibull distribution has maximum passing rate of the K-S and  $\chi^2$  tests in both scenarios.

## Acknowledgements

The authors would like to express their sincere thanks to the staffs of the Communication Technology and Type Approval Lab for their contributions during the measurement campaign. This work was supported by Iran Telecommunication Research Center under contract number 500/8844.

## References

- [1] ADAMS, J. C., GREGORWICH, W., CAPOTS, L., LICCARDO, D. Ultra-wideband for navigation and communications. In *Proc. of IEEE Aerospace Conference*, 2001, vol. 2, p. 785–792.
- [2] GEZICI, S., SAHINOGLU, Z., KOBAYASHI, H., POOR, H. V. Ultra-wideband impulse radio systems with multiple pulse types. *IEEE J. Sel. Areas Commun.*, 2006, vol. 24, no. 4, p. 892–898.
- [3] ARSLAN, H., CHEN, Z. N., DI BENEDETTO, M.-G. *Ultra Wideband Wireless Communications*, John Wiley & Sons, 2006.
- [4] GHASSEMZADEH, S. S., JANA, R., RICE, C. W., TURIN, W., TAROKH, V. Measurement and Modeling of an Ultra-Wide Bandwidth Indoor Channel. *IEEE Trans. Commun.*, 2004, vol. 52, no.10, p. 1786–1796.
- [5] CICCIGNANI, W., DURANTINI A., CASSIOLI, D. Time domain propagation measurements of the UWB indoor channel using PN-sequence in the FCC-compliant band 3.6–6 GHz. *IEEE Trans. Antennas Propag.*, 2005, vol. 53, no. 4, p. 1542–1549.
- [6] MUQAIBEL, A., SAFAAI-JAZI, A., ATTIYA, A., WOERNER, B., RIAD, S. Path-loss and time dispersion parameters for indoor UWB propagation. *IEEE Trans. Wirel. Commun.*, 2006, vol. 5, no. 3, pp. 550–559.
- [7] HENTILÄI, L., TAPARUNGSSANAGORN, A., VIITTALA, H., HÄMÄLÄINEN, M. Measurement and modelling of an UWB Channel at hospital. In *Proc. of IEEE Int. Conf. on Ultra-Wideband*, 2005, p. 113–117.
- [8] MOLISCH, A. F., CASSIOLI, D., CHONG, C.-C., EMAMI, S., FORT, A., KANNAN, J., KAREDAL, J., KUNISCH, B., SCHANTZ, H. G., SIWIAK, K., WIN, M. Z. A. Comprehensive Standardized Model for Ultrawideband Propagation Channels. *IEEE Trans. Antennas Propag.*, 2006, vol. 54, no. 11, p. 3151–3166.
- [9] MUQAIBEL, A. H. *Characterization of Ultra Wideband Communication Channels*. 2003, Ph.D. Dissertation, ECE Dept. at Virginia Tech.
- [10] RAPPAPORT, T. S. *Wireless Communications: Principles and Practice*. 2nd ed. Prentice Hall, 2002.
- [11] RAPPAPORT, T. S. Characterization of UHF multipath radio channels in factory buildings. *IEEE Trans. Antennas Propag.*, 1989, vol. 37, no. 8, p. 1058–1069.
- [12] FOERSTER, J. R., LI, Q. *UWB Channel Modeling Contribution from Intel*. Intel Corporation, Hillsboro, OR, USA, Techn. Report P802.15 02/279 SG3a, IEEE P802.15 SG3a contribution, 2002.
- [13] CHONG, C.-C., YONG, S. K. A generic statistical based UWB channel model for high-rise apartments. *IEEE Trans. Antennas Propag.*, 2005, vol. 53, no. 8, p. 2389–2399.
- [14] SALEH, A. A. M., VALENZUELA, R. A. A statistical model for indoor multipath propagation. *IEEE J. Sel. Areas Commun.*, 1987, vol. 5, no. 2, p. 128–137.
- [15] MOLISCH, A. F., KANNAN, B., CHONG, C.-C., EMAMI, S., FORT, A., KAREDAL, J., KUNISCH, J., SCHANTZ, H., SCHUSTER U., SIWIAK, K. *IEEE 802.15.4a channel model—final report*. IEEE 802.15-04-0662-00-004a, 2004.
- [16] HENTILÄI, L., TAPARUNGSSANAGORN, A., VIITTALA, H., HÄMÄLÄINEN, M. Measurement and modelling of an UWB Channel at hospital. In *Proc. of IEEE Int. Conf. on Ultra-Wideband*, 2005, p. 113–117.
- [17] FOERSTER, J. R., LI, Q. *UWB Channel Modeling Contribution from Intel*. IEEE P802.15-02/279r0-SG3a, 2002.
- [18] LI Q., WONG, W. S. Measurement and analysis of the indoor UWB channel. In *Proc. of IEEE Vehicular Technologies Conf. (VTC 2003-Fall)*, 2003, pp. 1–5.
- [19] CASSIOLI, D., WIN, M. Z., MOLISCH, A. F. The ultra-wide bandwidth indoor channel: from statistical model to simulations. *IEEE J. Sel. Areas Commun.*, 2002, vol. 20, no. 6, pp. 1247–1257.
- [20] ZHU, F., WU, Z., NASSAR, C. R. Generalized fading channel model with application to UWB. In *Proc. of IEEE Conf. UWB Systems and Technologies*, 2002, p. 13–18.
- [21] KUNISCH J., PAMP, J. Measurement results and modeling aspects for the UWB radio channel. In *Proc. of IEEE Conf. UWB Systems and Technologies*, 2002, p. 19–23.
- [22] ALVAREZ, A., VALERA, G., LOBERIA, M., TORRES, R., GARCIA, J. L. Ultrawideband channel characterization and modeling. In *Proc. of Int. Workshop on Ultra Wideband Systems (IWUWBS 2003)*, 2003.
- [23] PAGANI P., PAJUSCO, P. Experimental assessment of the UWB channel variability in a dynamic indoor environment. In *Proc. of IEEE Int. Symp. on Personal, Indoor and Mobile Radio Communications (PIMRC 2004)*, 2004, pp. 2973–2977.

## About Authors

**Narges NOORI** (B. Sc. 1998, M. Sc. 2000, Ph. D. 2006 degrees (with honors) from Iran University of Science and Technology (IUST), Tehran, Iran, all in Electrical Engg.) was with RF/Microwave and Photonics Group, Univ. of Waterloo, Ontario, Canada as a visiting scholar (2004 to 2005). In 2005, she joined Iran Telecommunication Research Center (ITRC), Tehran, Iran, now as a research assistant professor. In 2008, she received the Best Researcher Award from Ministry of Communication & Information Technology (ICT) of Iran. Her research interests include radio propagation and channel modeling, broadband and ultra wideband communications, and numerical methods in electromagnetics.

**Roghieh KARIMZADEH BAEE** (B. Sc. from Khaje Nasir Al-Deen Toosi Univ. (KNTU), Tehran, Iran, in 2001, M. Sc. from Urmia Univ., Iran, in 2003, both in Commun. Engg.) joined ITRC as a Researcher in Radio Commun. Group in 2003. She is currently working toward the Ph.D. degree at the El. and Computer Engg. Dept. of Tarbiat Modares Univ., Tehran, Iran. Her research interests include propagation channel modeling, design and analysis of practical antennas, phase array antenna, metamaterials and passive microwave devices.

**Ali ABOLGHASEMI** (B. Sc. 1991, M. Sc. 1995, both in El. and Telecommun. Engg. from KNTU, Tehran, Iran) worked on switching and signaling in fixed and mobile communication system (1997 to 2007). He is now a faculty member in Radio Communication group of ITRC. His research interests include wireless communication systems, especially ultra wideband, 3G and mobile communications.